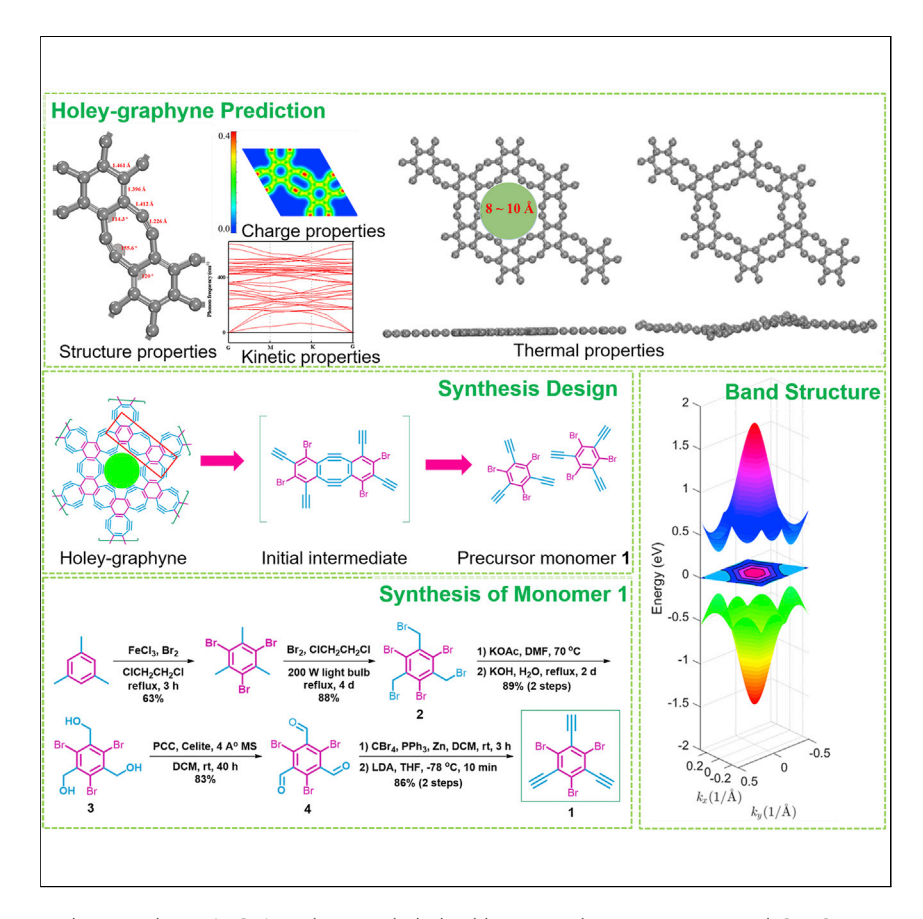
Matter



Article

Constructing two-dimensional holey graphyne with unusual annulative π -extension



Holey graphyne (HGY) is alternately linked between benzene rings and $C \equiv C$ bonds and is composed of six-vertex and highly strained, eight-vertex rings and an equal percentage of sp^2 and sp hybridized carbon atoms. Density functional theory (DFT) has proven its stability of thermodynamic, kinetic, mechanical, and thermal properties; thus, it is a promising synthetic target. We report HGY synthesized in an interfacial, two-solvent system through a Castro-Stephens-type coupling reaction from 1,3,5-tribromo-2,4,6-triethynylbenzene. DFT predicted HGY is a p-type semiconductor with a direct bandgap (\sim 1.1 eV) and high carrier mobility.

Xinghui Liu, Soo Min Cho, Shiru Lin, ..., Eun Hee Baek, Do Hyun Ryu, Hyoyoung Lee

dhryu@skku.edu (D.H.R.) hyoyoung@skku.edu (H.L.)

Highlights

A two-dimensional carbon allotrope of holey graphyne (HGY) was designed

1,3,5-tribromo-2,4,6triethynylbenzene was synthesized for fabrication of HGY

HGY comprised a pattern of sixvertex and highly strained, eightvertex rings

HGY's direct p-type semiconductor with high carrier mobility was simulated



Liu et al., Matter 5, 1–13 July 6, 2022 © 2022 Elsevier Inc. https://doi.org/10.1016/j.matt.2022.04.033

Matter



Article

Constructing two-dimensional holey graphyne with unusual annulative π -extension

Xinghui Liu,^{1,2,6} Soo Min Cho,^{2,6} Shiru Lin,³ Zhongfang Chen,³ Wooseon Choi,⁴ Young-Min Kim,⁴ Eunbhin Yun,^{1,2} Eun Hee Baek,² Do Hyun Ryu,^{2,*} and Hyoyoung Lee^{1,2,5,7,*}

SUMMARY

Here, we report two-dimensional, single-crystalline holey graphyne (HGY) synthesized in an interfacial two-solvent system through a Castro-Stephens-type coupling reaction from 1,3,5-tribromo-2,4,6-triethynylbenzene. As a new type of 2D carbon allotrope, HGY is alternately linked between benzene rings and C≡C bonds and is composed of a pattern of six-vertex and highly strained, eight-vertex rings and an equal percentage of sp² and sp hybridized carbon atoms. By combining experimental and theoretical studies, we systematically investigated the stability of HGY and its vibrational and optical properties. Density functional theory computations predicted that HGY is a p-type semiconductor that embraces a direct bandgap (~1.1 eV) with a high carrier mobility. Transmission electron microscopic studies revealed that the synthesized HGY sheets are highly crystalline with AB stacking. Its semiconducting character, nonlinear sp bonding, and special π -conjugated structure endow HGY with promising applications in optoelectronic, energy harvesting, gas separation, catalysis, water remediation, sensor, and energy-related fields.

INTRODUCTION

Diamond and graphite are two naturally occurring carbon allotropes, which possess sp³ and sp² hybridized carbon atoms, respectively. The discovery of various other carbon allotrope materials, such as graphene, fullerene, carbon nanotube,³ graphyne,^{4–8} and graphdiyne,^{4–9} has been revolutionizing modern nanomaterials science. Graphyne, firstly predicated by Baughman et al. in 1987,⁵ is a new form of two-dimensional (2D) carbon material with sp and sp^2 carbon atoms. The presence of the sp carbon atoms (or acetylenic linkages) in graphyne disintegrates the original honeycomb lattice of graphene. Accordingly, unlike graphene with only a honeycomb lattice structure, graphynes can adopt many different geometries. So far, mainly four different geometries of graphynes, namely α -, β -, γ -, and 6,6,12-graphyne, ⁴⁻⁹ have been explored, and their percentages of acetylenic linkages are 100%, 66.67%, 33.33%, and 41.67%, respectively. Interestingly, similar to graphene, α -, β -, and 6,6,12-graphynes⁵ have Dirac-cone-like band structures at the Fermi level and exhibit small carrier effective masses and high carrier mobility,⁶ while graphdiyne⁴ and γ-graphyne⁵ possess nonzero band gaps. Recently, Casari and coworkers experimentally fabricated the graphdiyne-like carbon nanonetwork¹⁰ and designed all graphdiyne-related carbon allotropes, ¹¹ giving possible guidelines for designing new 2D carbon materials. The unique properties of graphynes make them strong competitors of graphene, at least for some applications.

Progress and potential

Carbon has many faces, such as graphene, nanotubes, fullerene, and graphdiyne, where hexagons are the primary building blocks of these materials. Since many of the exotic properties of carbon allotropes are related to their unique structure, some basic questions will occur. Is it possible to design new carbon allotropes? An intriguing molecule, dibenzocyclooctadiyne, first synthesized by Sondheimer and coworkers, caught our attention. In dibenzocyclooctadiyne, two aromatic benzene rings are connected by two bent acetylenic linkages, resulting in a highly strained, eight-membered ring. This interesting molecule inspired us to design and synthesize the new carbon allotrope, namely holey graphyne, as reported in this work.





Graphene research has made significant advances in modern chemistry and physics because of its fascinating properties. 1,6,12 However, the zero-bandgap electronic structure of graphene limits its application for semiconducting materials. Therefore, it is necessary to find new types of 2D carbon allotropes that have exceptional semiconducting properties, such as a proper energy bandgap and high mobility. Comparing graphene, 12 γ -graphyne, 5 and graphdiyne, 5,8,9 we can expect that 2D carbon allotropes constructed by alternatively linking sp^2 benzene rings and sp acetylenic chains with an appropriate sp^2/sp bonding ratio may help design the holey graphyne (HGY), an ideal 2D semiconducting material. An intriguing molecule, dibenzocyclooctadiyne, firstly synthesized by Sondheimer and coworkers in 1974, 13 caught our attention. In dibenzocyclooctadiyne, two aromatic benzene rings are connected by two bent acetylenic linkages, resulting in a highly strained, eightmembered ring. This exciting molecule inspired us to design and synthesize the new carbon allotrope, namely HGY, as reported in this work.

Herein, we report a new type of carbon allotrope, HGY, whose structure is composed of a pattern of hybridized six-vertex and eight-vertex rings. We synthesized the ultrathin, single-crystalline HGY by the bottom-up approach through a transition-metal-mediated cross-coupling from 1,3,5-tribromo-2,4,6-triethynylbenzene in the interface of two-solvent system (water and dichloromethane). We systematically investigated its stability and spectroscopic and electronic properties by joint experimental and theoretical studies. It is revealed that HGY may have promising potential applications in optoelectronic and energy-related fields.

RESULTS AND DISCUSSION

Structure and stability of HGY by DFT computations

By means of density functional theory (DFT) computations, we theoretically investigated the geometric structure of HGY and its stability (see Data S1. Crystallographic information files of HGY). HGY, the novel carbon allotrope, has a space group P6/ mmm (D_{6h}^{-1}) in the Hermann-Mauguin (Schoenflies) notation. Different from graphene with only six-membered carbon rings, HGY not only has six-membered rings but also has eight-membered carbon atom rings between the hexagonal units (Figure 1A). The optimized lattice constant is a = b = 10.83 Å (Figure S1; Tables S1–S3). According to bonding analysis (Figure 1A), the carbon atoms in six-membered rings are sp^2 hybridized, and these rings have alternating single and double bonds with the bond distance of 1.461 and 1.396 Å, respectively. In comparison, the carbon atoms in the eight-membered rings are sp hybridized; the bond lengths in these rings are alternate as 1.461, 1.412, and 1.226 Å; and the angles are alternate as 114.3° and 155.6°, respectively (Figure 1A). Note that these bonds have different charge densities (Figure 1B), and the variation in bond charge density indicates the different types of carbon bonding (sp^2 and sp). These charge density results are also in good agreement with the line charge density along the lattice direction (Figure S2).

Stability is a primary requirement for real applications. The stability can be evaluated by the computed cohesive energy, phonon spectra, elastic constants, and *ab initio* molecular dynamics (AIMD) simulations. First, the cohesive energy per atom, E_{coh} , is calculated by $E_{coh} = (n \cdot E_{coh}, a_{tom} - E_t)/n$, where E_{coh} , a_{tom} , E_t , and n are the total energy of the carbon atom, the total energy of the primitive cell, and the number of carbon atoms per primitive cell. The cohesive energy of HGY (7.30 eV/atom) is very close to that of graphene (8.11 eV¹), indicating its good thermodynamic stability. Then, we calculated the phonon frequencies of HGY for all modes in the Brillouin

https://doi.org/10.1016/j.matt.2022.04.033

¹Center for Integrated Nanostructure Physics (CINAP), Institute of Basic Science (IBS), 2066 Seoburo, Jangan-Gu, Suwon 16419, Republic of Korea

²Department of Chemistry, Sungkyunkwan University (SKKU), 2066 Seoburo, Jangan-Gu, Suwon 16419, Republic of Korea

³Department of Chemistry University of Puerto Rico, Rio Piedras Campus, San Juan, PR, USA

⁴Department of Energy Science, Sungkyunkwan University (SKKU), 2066 Seoburo, Jangan-Gu, Suwon 16419, Republic of Korea

⁵Department of Biophysics, Sungkyunkwan University (SKKU), 2066 Seoburo, Jangan-Gu, Suwon 16419, Republic of Korea

⁶These authors contributed equally

⁷Lead contact

^{*}Correspondence: dhryu@skku.edu (D.H.R.), hyoyoung@skku.edu (H.L.)



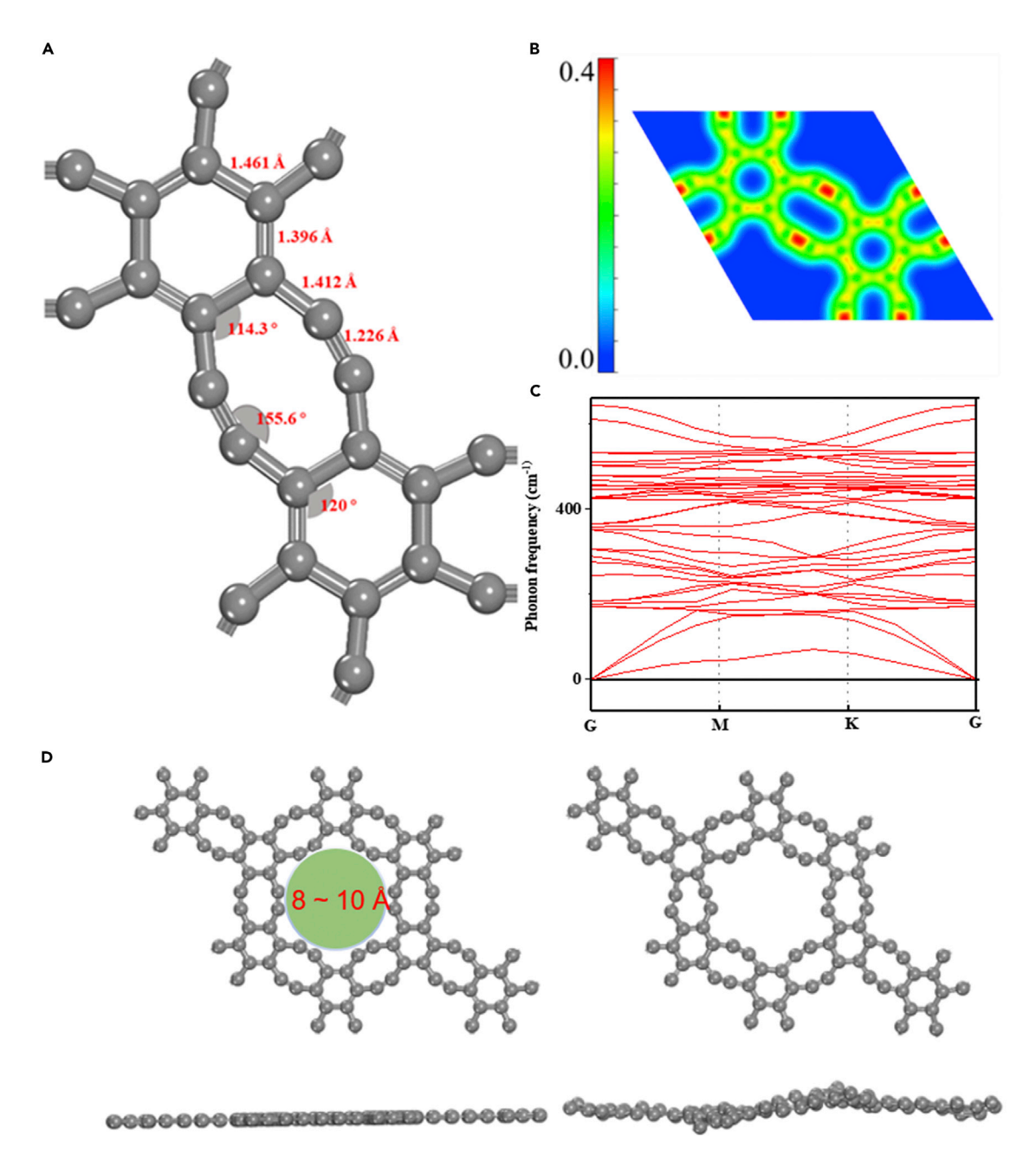


Figure 1. Structure and stability properties of the HGY sheet

- (A) The illustration of the primitive cell structure of HGY that shows detailed bonding information.
- (B) The electronic charge density contours corresponding to the unit cell.
- (C) The phonon band structures of HGY without imaginary frequency.
- (D) Snapshots of trajectories for HGY (2*2*1 supercell) monolayer at 1,000 K, following a 10-ps AIMD simulation: before and after. For the full structure information of HGY, see Data S1: Crystallographic information files of HGY.

zone (BZ) (Figures 1C and S2). No imaginary frequencies were observed, which indicates that HGY is kinetically stable. Note that the maximum frequency of the longitudinal optic mode (LO) is as high as 2,400 cm $^{-1}$ in the carbon chain. 2 In addition, the elastic constants of HGY (C $_{11}$ = C $_{22}$ = 91.06 N/m, C $_{12}$ = 35.60 N/m, and C $_{66}$ = 0.15 N/m) satisfy the specification for hexagonal 2D crystal (C $_{11}$ > |C $_{12}$ |, C $_{66}$ > 0), showing that HGY is mechanically stable.





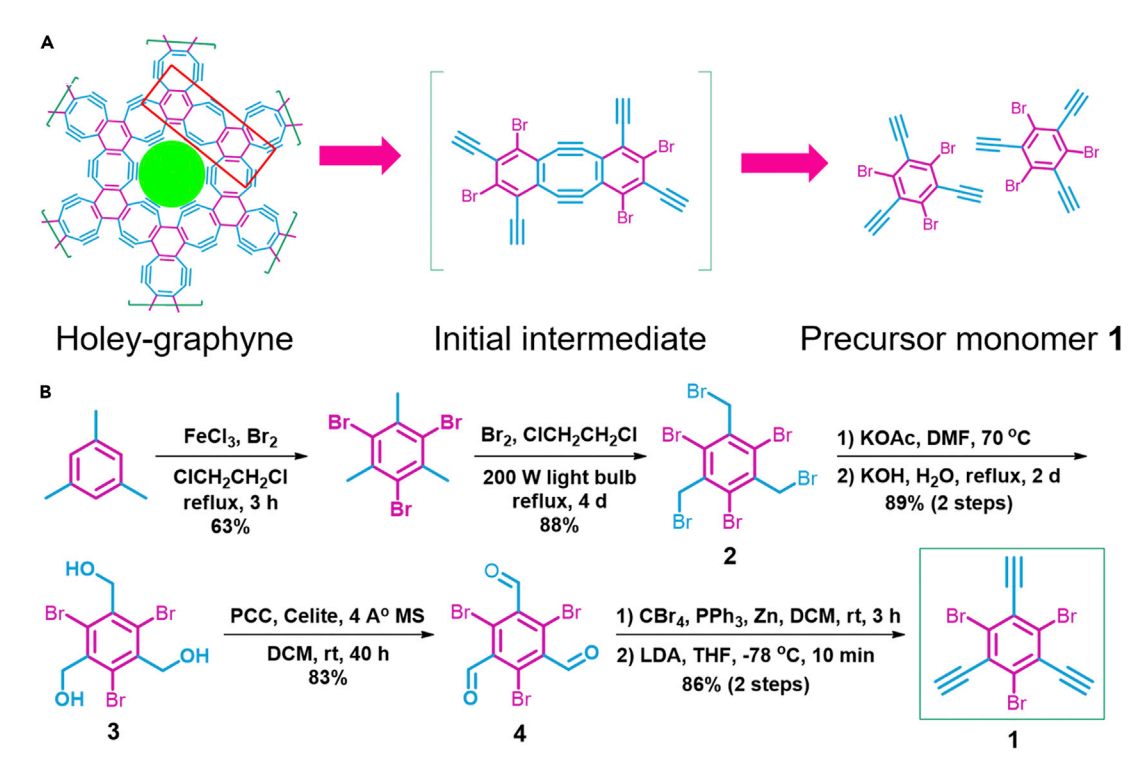


Figure 2. Synthetic scheme of HGY

(A) Rational design of synthetic scheme of HGY by precursor monomer 1,3,5-tribromo-2,4,6-triethynylbenzene using transition-metal-mediated cross-coupling reaction.

(B) Synthetic scheme of precursor monomer 1,3,5-tribromo-2,4,6-triethynylbenzene (1).

To further investigate the issue of thermal stability, we carried out AIMD simulation at T = 1,000 K for 10 ps. Comparing the atomic structures (2*2*1) before and after the AIMD simulation (Figure 1D), it is found that HGY remains as a well-connected framework after 10 ps of MD simulations at this high temperature, indicating its good thermal stability. Our experimental thermogravimetric analysis (TGA) showed that the decomposition temperature of HGY is about 750°C (Figure S2), which is consistent with the AIMD simulations. The above results strongly indicate that HGY is of good thermodynamic, kinetic, mechanic, and thermal stabilities and thus a promising synthetic target.

Experimental synthesis of HGY

To synthesize HGY, we designed a synthetic scheme by Castro-Stephens-type coupling reaction using a new monomer (1,3,5-tribromo-2,4,6-triethynylbenzene, 1) (Scheme S1; Figures 2A and 2B). Firstly, we synthesized the known 2,4,6-tribromobenzene-1,3,5-tricarbaldehyde 4 (the precursor of 1) from mesitylene by modified literature procedure. Then, 1 was synthesized from 4 using Corey-Fuchs reaction with lithium diisopropylamide as a base. More specifically, to illustrate the preparation of monomer 1 of HGY, the detailed reaction procedures (H nuclear magnetic resonance [NMR], NMR spectra, the reaction yields, and detailed process) are given in supplemental information (Figures S3–S9). Finally, monomer 1 was transformed into the crystalline HGY film on the interface between the organic and water phases via the initial intermediate (Figures 2A and S10). The synthesized HGY was identified using NMR (Figure S9), which shows four prominent peaks. The two peaks at 91.1 (red color) and 80.9 ppm (blue color) are assigned to the sp

Please cite this article in press as: Liu et al., Constructing two-dimensional holey graphyne with unusual annulative π -extension, Matter (2022), https://doi.org/10.1016/j.matt.2022.04.033





carbon atoms, whereas the two peaks at 129.7 and 126.8 ppm are attributed to the sp^2 carbon (green color). Note that the 91.1 ppm is the newly formed sp bonding, and the 80.9 ppm peak is the terminal (defect) sp bonding.

To gain insights into the underlying mechanism for the formation of strained HGY from the initial dimer intermediate rather than the initial trimer intermediate, we applied the climbing-image nudged elastic band (CI-NEB) method to evaluate the energy barrier of both modes (Figure S11). Both reactions are exothermic, according to the energy profiles from the initial states to the final states of dimer and trimer. However, the energy barrier for dimer formation (17.76 eV) is lower than trimer formation (23.74 eV), which further confirms the design of the HGY formation process, and ruled out the formation of the 2D (γ -graphyne) structure based on trimer intermediate. Note that HGY can be formed at room temperature in comparison with γ -graphyne, since the difference between both energy barriers is 5.98 eV, indicating the γ -graphyne needs more energy than HGY for overcoming the kinetic energy barrier.

Characterization of morphologies and structures

The morphologies of HGY, with the lateral dimension up to several micrometers, were characterized by optical microscopy (OM) and scanning electron microscopy (SEM) (Figure 3A). The flat sheet with a thickness of 5.3 nm was observed by atomic force microscopy (AFM) (Figure 3B) and the 3D image of the HGY film (Figure S12), which may be about 15 layers of HGY since the interlayer distance is about 0.36 nm (based on the transmission electron microscopy [TEM] measurements described below). The TEM was used further to analyze the morphology and microstructure of the 2D film: both the low-resolution TEM image (Figure \$13) and the high-resolution TEM (HRTEM) image (Figure 3C) reconfirm the successful synthesis of a continuous film. The corresponding fast Fourier transform (FFT) pattern of the HRTEM image (inset Figure 3C) verifies the single-crystalline nature of the film, which means that the structure of the film has significant in-plane order over a relatively large area and exhibits the single-crystal diffractions spots. The d-spacing along the (200) reflections of HGY is 0.442 nm (Figure 3D). Another set of hexagonally arranged diffraction spots with a larger d-spacing of 0.27 nm was also observed, which can be indexed by the (220) reflections of HGY.

To further verify the crystal structure of the nanosheet, we simulated HRTEM along [001] zone axis observation using the optimized HGY model with "AB" stacking mode at a different thickness (t) (ranging from 1.3 to 61.4 nm with a step of 10 nm) and defocus (Δf) ranging from -120 to +240 nm with a step of 60 nm) (Figures 3E and S14). The simulated HRTEM images with a large value range Δf (120–240 nm) well match the experimental images (the green and red squares; Figures 3D and 3E). Thus, we expect that the HGY nanosheets are stacked in the "AB" manner. Furthermore, we examined the crystal structure of the HGY by X-ray diffraction (XRD) measurement. The (002) peak at approximately 24.5° for HGY indicates an interlayer spacing of 0.36 nm (Figure 3F), consistent with the FFT pattern of Figure 3G. Note that the lattice fringe image of HRTEM reveals curve streaks with a lattice parameter of 0.36 nm, in agreement with the XRD result of the (002) peak, indicating the spacing between carbon layers (Figures 3H–3J). The interlayer spacing value (\sim 0.36 nm) between HGY layers is slightly higher than that of graphene due to the weak van der Waals interactions. $^{17-19}$

Spectroscopic characterization

The study of spectroscopic properties^{20–22} is essential for the new carbon allotropes of HGY. The elemental composition and bonding structure were probed



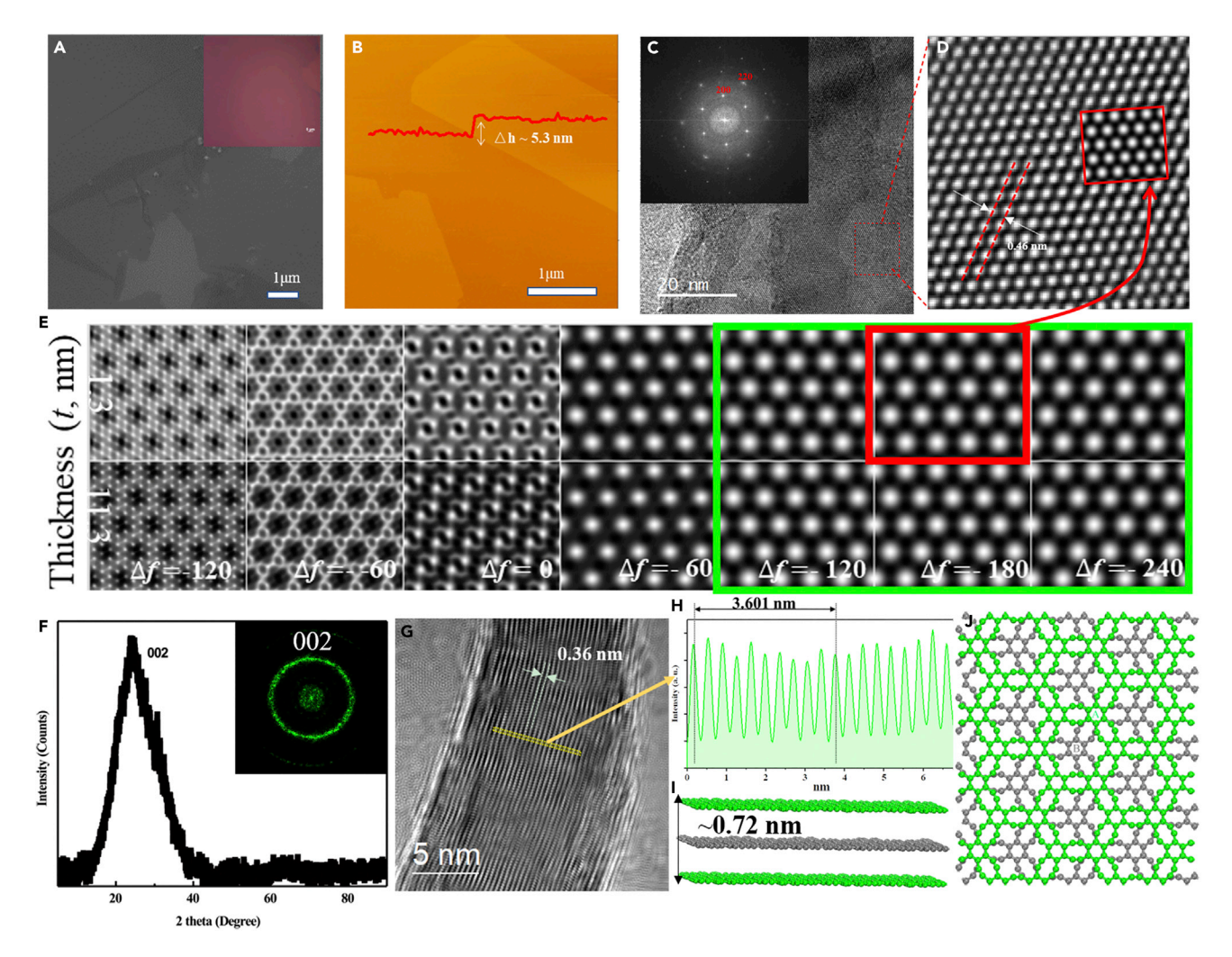


Figure 3. The morphologies and structure characterization of HGY film

- (A) SEM image and optical microscopy (OM) image (inset) of HGY.
- (B) AFM image of HGY on Si/SiO₂ substrate.
- (C) High-resolution TEM (HRTEM) image of HGY. Related fast Fourier transform (FFT) results patterns are in corresponding insets.
- (D) Enlarged inverse FFT (IFFT) image of the area highlighted by the red square (Figure 2C) and simulated projected potential map with "AB" stacking mode (inset the red square). The more detailed information is displayed in Figure \$14.
- (E) Simulated HRTEM images of HGY by "AB" stacking mode with different thickness (t) and different defocus (Δf) along the [001] zone axis. The unit of the t and Δf values is nm. The result is given that the simulated HRTEM image with large values range Δf (120–240 nm) of over-focus is in agreement with the experiment and filtering HRTEM images, which are showing by the red square and contrast pattern of HRTEM is less sensitive to the change of thickness for the stacked sample.
- (F) The crystal structure of the HGY was examined by X-ray diffraction (XRD) and the FFT patterns of Figure 2G (inset), which are consistent with each other.
- (G) The lattice fringe of an HRTEM image of HGY reveals curve streaks with the lattice parameter of 0.36 nm and agreement with the XRD pattern shown in Figure 2E.
- (H) The line profiles from the green line indicate that the interlayer spacing between HGY layers is 0.36 nm.
- (I and J) The mode is corresponding to the (I) side view and (J) top view of the "AB" stacking of bi-layer HGY, respectively, which is the structure of the HRTEM simulations.

systemically with energy-dispersive X-ray spectroscopy (EDS), X-ray photoelectron spectroscopy (XPS), Fourier-transform infrared spectroscopy (FT-IR), and Raman spectroscopy. The survey spectra of XPS (Figures 4A and S15) indicate that HGY is composed primarily of elemental carbon, with silicon and oxygen signals from the underlying SiO_2 layer. The corresponding scanning transmission electron





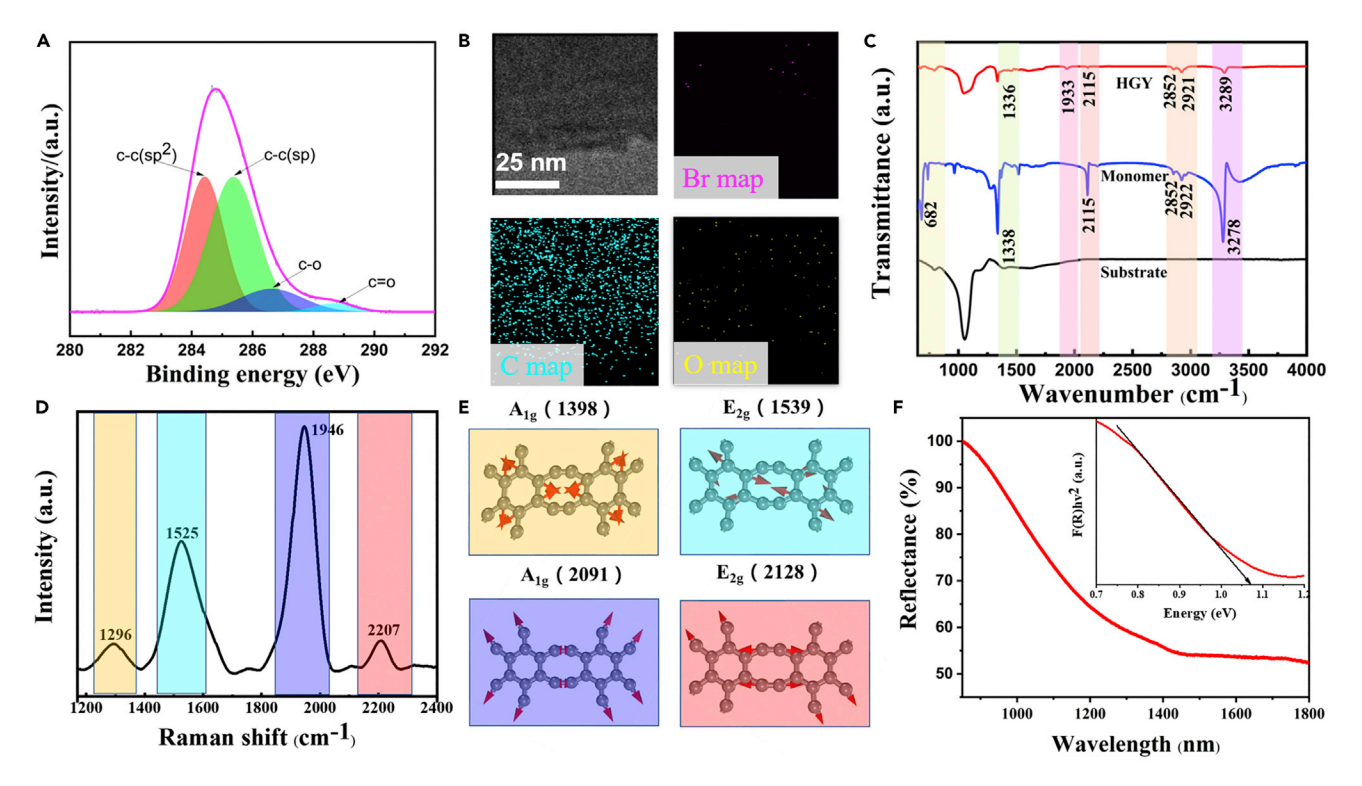


Figure 4. Spectroscopic characterization of HGY

- (A) High-resolution core-level XPS spectrum of C 1s of HGY indicates the sp/sp^2 ratio is 1.
- (B) STEM-EDS element mapping images of HGY show that the HGY film is composed mainly of elemental carbon.
- (C) FT-IR spectra of HGY, monomer 1, and substrate.
- (D) Dominated Raman spectra of HGY obtained from the experimental measurement, which is associated with the newly formed sp peak (the excitation wavelength is 532 nm).
- (E) The simulation atomic displacements of A_{1g} and E_{2g} Raman vibration modes for sp and sp^2 , obtained from the DFT simulation. The four Raman active vibration models correspond to the four dominating Raman peaks in (D).
- (F) Diffuse reflectance spectrum and transformed Kubelka-Munk spectra of HGY shows \sim 1.07 eV.

microscopy (STEM)-EDS maps (Figure 4B) show the distributions of C, Br, and O. As a result, carbon is the dominating element in the film, proving the high completion of transition-metal-mediated cross-coupling reaction to give 2D HGY nanosheets. The electron image and EDS (Figure S16) analysis are consistent with the XPS result. High-resolution XPS can discriminate against the circumstance of an element. The C 1s peak at 284.8 eV is deconvoluted into four Gaussian sub-peaks (Figure 4A), which are mainly contributions by sp^2 (C=C; at 284.5 eV) and sp (C \equiv C; at 285.3 eV) species. Also, the abundance ratio of the sp/sp^2 carbon is 1, the same as the chemical composition analysis of the HGY structure. The sub-peaks C-O and C=O, with minor contributions to the C 1s peak, are located at 286.6 and 288.5 eV, respectively. The presence of elemental O most likely derives from the absorption of air in the pores and the oxidation of terminal alkyne, which will cause some defects.

Meanwhile, we analyzed the FT-IR spectroscopy of HGY and compared with that of monomer 1. When the 2D crystalline HGY is formed, the C–Br stretching (at $682 \, \mathrm{cm}^{-1}$) and the C \equiv C–H stretching (at $3,278 \, \mathrm{cm}^{-1}$) in monomer 1 both dramatically decrease (to nearly negligible). The peak C \equiv C stretching modes (Figure 4C) were identified at $1,933 \, \mathrm{cm}^{-1}$ and $2,115 \, \mathrm{cm}^{-1}$ for HGY and 1, respectively. Note that the peak at $1,933 \, \mathrm{cm}^{-1}$ corresponds to the newly formed C \equiv C (sp) bonds due to the coupling reaction of 1. The intense stretching of the carbon rings





(1,336 cm⁻¹ in HGY; 1,338 cm⁻¹ in 1) indicates the in-plane bending vibration of delocalized benzene rings of HGY, confirming the structure of HGY. Raman scattering spectroscopy is a powerful tool to analyze the structural information of HGY, particularly for those Raman-active alkyne linkers arrayed in the concrete topology of HGY. Thus, we measured the Raman spectrum of HGY and assigned the vibration modes by comparing it with the DFT-simulated spectrum (Figures 4D and 4E). Experimentally, all the Raman active peaks are in the range of 200 cm⁻¹ to 2,500 cm⁻¹, which agrees with the computational results (Figures S17-S19). The two prominent peaks of $C \equiv C$ (sp) at 1,946 cm⁻¹ and 2,207 cm⁻¹ in the measured Raman spectrum are assigned to the A_{1g} (2,091 cm⁻¹) and E_{2g} (2,128 cm⁻¹) vibration modes of sp bonding (Figure 4E) in the conjugated alkyne linkage (Figure 4C). The experimentally observed peak at 1,525 cm⁻¹ corresponds to the first-order scattering of the E_{2g} (1,539 cm $^{-1}$) vibration mode for the in-phase stretching of sp² carbon, which is red shifted compared with the G band of graphite (1,575 cm⁻¹).²³ The measured 1,296 cm⁻¹ peak, called the D band, corresponds to the breathing A_{1q} vibration (1,398 cm⁻¹) of sp^2 carbon domains in aromatic rings (see supplemental experimental procedures for details). Terminal alkyne vibrational modes (2,100-2,120 cm⁻¹) are almost negligible, indicating that most of the terminal alkyne residues of monomers were integrated into the π -conjugated network of HGY,²⁴ except for a few edges and defect sites.

Electronic properties characterization

The bandgap (E_g) is an essential feature of semiconductors that determines their applications in optoelectronics. Here, diffuse reflectance spectroscopy (DRS) is used to investigate the bandgap of HGY. From the reflectance spectrum of HGY, the optic absorption coefficient (α) was obtained (Equation S1) from the Kubelka-Munk equation (Equation S2). The bandgap of the HGY is determined to be \sim 1.1 eV based on the direct transition from the Kubelka-Munk function (Figure 4F), which is consistent with the calculated bandgap (~1.0 eV) from the electronic structure (Figures 5A and 5B) and of HGY by DFT simulation via using HSE06 function. Note that HGY is a p-type semiconductor material with a direct bandgap of 1.1 eV at the K point (Figure 5B) in the reciprocal lattice of the primitive cell. The conduction band minimum (CBM) and the valence band maximum (VBM) originate from the π^* and π band states, respectively, and the band dispersion arises mainly from the overlap of the carbon 2Pz orbitals (Figure 5C). In addition, the wavefunction of a pair of orbitals at the K point of CBM and VBM is plotted (Figure 5D).²⁵ More details of the electric structure and work function (5.2 eV) are presented in Figures S20 and S21 and supplemental experimental procedures.

The first Brillouin zone (FBZ) (Figure 5E) is related to the hexagonal (red line) and orthogonal (blue line) lattice. The K point (fractional k-space coordinates [-1/3, 2/3, 0]) defined in the reciprocal lattice of the primitive hexagonal cell is folded into (0, 1/3, 0) point sitting at a direction in the FBZ of the orthogonal supercell. Compared with the rhombus drawn with dashed lines (Figure 5F), there are 48 atoms in this rectangle drawn with dashed lines (lattice constants $a_{ox} = 18.76$ Å and $b_{oy} = 10.83$ Å).

Bardeen and Shockley in 1950^{26} derived the deformation potential (DP) theory for intrinsic carrier mobility (u) of the non-polar crystal, which has been extensively applied to study mobility (μ) in 2D materials. ^{25,27–29} In this charge transport calculation, we adopted the orthogonal supercell along with two vertical directions, x and y, for the HGY sheet, which allows for a more intuitive explanation for the transport property (Figures 5G and S22).

Matter Article

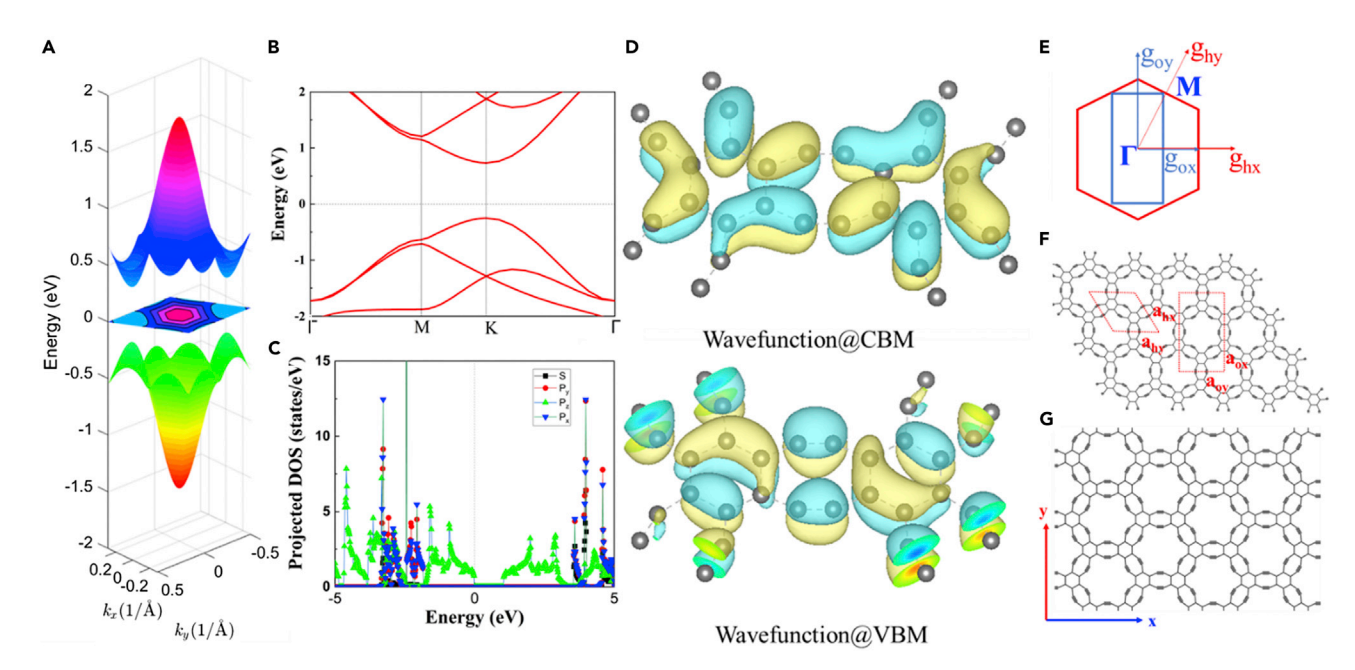


Figure 5. Electronic property characterization of monolayer HGY sheet

- (A) Three-dimensional (3D) electronic band structure of HGY.
- (B) The band structures
- (C) Partial density of states of HGY by HSEO6 functional.
- (D) K point degenerate valence band maximum wave function (Wavefunction@VBM) and conduction band minimum wave function (Wavefunction@CBM) for HGY.
- (E) The first Brillouin zone (FBZ) is associated with the two lattices. The blue line shows the folding of the K point in FBZ of the hexagonal lattice into FBZ related to the orthogonal lattice.
- (F) Atomic structure model of monolayer HGY. The dashed lines represent the primitive hexagonal cell (defined by a_{hx} and a_{hy}) and the orthogonal supercell (defined a_{ox} and a_{oy}).
- (G) The orthogonal supercell is defined as the \boldsymbol{x} and \boldsymbol{y} directions for the mobility calculation.

Based on DP theory, deformation potential (E_1) , elastic moduli (C), effective mass (m^*) , and relaxation time (τ) using Equation S3 were obtained (see supplemental experimental procedures for details). The calculated mobility and the relaxation time are calculated and summarized in Table 1. To compare with other 2D carbon allotropes, the relaxation times, mobilities, bandgaps of α -, β -, 6-6-12-graphyne, graphene, and graphdiyne were presented in Table S4.^{25,29} Note that the effective mass of 0.15 m_e along with the x direction is lower than that of 0.21 m_e along with the y direction, which can be attributed to the band dispersed along the x direction being more robust compared with the y direction. Specifically, the obtained intrinsic electron mobility is 1.16 \times 10⁴ cm² V⁻¹ s⁻¹ along with the x direction and 0.81 \times 10⁴ cm² V⁻¹ s⁻¹ along with the y direction. Note that the hole mobility along with x direction $(4.51 \times 10^4 \text{ cm}^2 \text{ V}^{-1} \text{ s}^{-1})$ and along with the y direction $(2.26 \times 10^4 \text{ cm}^2 \text{ V}^{-1} \text{ s}^{-1})$ is approximately three times higher than the mobility of the electrons. Based on the Equation S3, in comparison with the mobility of electrons, the high mobility of the holes in HGY can be attributed to the long, acoustic, phonon-scattering relaxation times. More specifically, the high hole mobility is mainly due to a small DP constant, indicating the coupling capability between the electron (hole) with the acoustic phonon. The electron at CBM may be more strongly coupled with the acoustic phonon than the holes at VBM, explained by the frontier molecular orbitals accountable for charge transport. As a result, the band edge shift (VBM and CBM) is exhibited as a function of strain (Figure S22), respectively. Also, the real space wave functions of VBM and CBM orbitals at the K point (Figure S22) are consistent with frontier molecular orbital theories, since

Please cite this article in press as: Liu et al., Constructing two-dimensional holey graphyne with unusual annulative π -extension, Matter (2022), https://doi.org/10.1016/j.matt.2022.04.033





Table 1. The intrinsic mobility from the deformation potential (DP) theory					
Carrier type	E ₁ (eV)	C ^{2D} (N/m)	m* (m _e)	$\mu (10^4 \text{ cm}^2 \text{V}^{-1} \text{s}^{-1})$	τ(ps)
e ^y	1.91	91.06	0.21	0.81	0.96
h ^y	1.14	91.06	0.21	2.26	2.70
e ^x	1.89	91.06	0.15	1.61	1.37
h×	1.13	91.06	0.15	4.51	3.84

The deformation potential (E₁), in-plane elastic constant (C^{2D}), effective mass (m*), mobility (μ), and relaxation time (τ) for the electron (e) and hole (h) along x and y direction in 2D monolayer HGY sheet at 300 K.

the nodes of CBM along the x and y directions are higher than those of VBM (see supplemental experimental procedures for details). The above findings can well explain why the hole mobility is higher than the electron mobility. However, experimental measurements of HGY, such as small-angle X-ray diffraction (SAXRD) and charge-carrier mobility of its devices, are almost impossible at the current stage due to the limited synthesis of the defect-free HGY, which will be reported elsewhere in the future.

Conclusions

In summary, ultrathin single crystalline HGY consisting of six- and eight-vertex rings pattern was synthesized from 1,3,5-tribromo-2,4,6-triethynylbenzene monomer that could be prepared in five steps from mesitylene. This newly developed 2D material, HGY, is formed by alternately linking between sp2 benzene rings and sp C \equiv C bonds and shows "AB" stacking in multi-layered structures as revealed via HRTEM images, which is a slightly larger intermolecular distance than graphene due to its weak van der Waals force. The big holey pore diameter of HGY is about 0.8-1.0 nm. The bandgap was measured with DRS-UV to give \sim 1.1 eV; the hole mobility $(4.51 \times 10^4 \text{ cm}^2 \text{ V}^{-1} \text{ s}^{-1})$ and electron mobility $(1.61 \times 10^4 \text{ cm}^2 \text{ V}^{-1} \text{ s}^{-1})$ along x direction and the hole mobility (2.26 \times 10⁴ cm² V⁻¹ s⁻¹) and electron mobility $(0.81 \times 10^4 \, \text{cm}^2 \, \text{V}^{-1} \, \text{s}^{-1})$ along y direction at room temperature were predicted by DP theory. The present study not only demonstrates the first synthesis of the ultrathin, single-crystalline HGY but also introduces a new concept for the design and synthesis of a new type of 2D carbon allotrope. With unique nonlinear sp bonding, HGY may have more room for studying in the physics mechanism field and may pave the way for synthesizing more HGY-related 2D nanocarbon materials.

EXPERIMENTAL PROCEDURES

Resource availability

Lead contact

Further information and requests for resources should be directed to and will be fulfilled by the lead contact, Hyoyoung Lee, e-mail (hyoyoung@skku.edu).

Materials availability

This study did generate new unique materials and reagents.

Data and code availability

The authors confirm that the data supporting the findings of this study are available within the article and its supplemental information. Crystallographic information files https://www.ccdc.cam.ac.uk/structures/Search?ccdc=2144573 are shown in Data S1. The data supporting the plots in this paper and the other findings of this study are available from the corresponding author upon reasonable request.

Synthesis of 2,4,6-tribromobenzene-1,3,5-tricarbaldehyde

To a freshly activated celite (1.2 g) and 4 Å molecular sieves powder (1.2 g) heated for 1 h at more than 150°C, pyridinium chlorochromate (3.0 g, 14 mmol, 7.0 equiv) was added





at room temperature, and solid reagents were melted by dried dichloromethane (DCM) (105 mL). Compound 3 (810 mg, 2.0 mmol, 1.0 equiv) was added at room temperature, and the reaction mixture was stirred for 40 h under argon atmosphere. The resulting mixture was filtrated through a short pad of silica with DCM to obtain desired product 4 (662 mg; 83% yield) as a white solid. The crude product was used without further purification in the next step. Analytical data are consistent with reported values.²⁸

Synthesis of monomer 1,3,5-tribromo-2,4,6-triethynylbenzene

To a freshly dried zinc powder (590 mg, 9.0 mmol, 12 equiv), tetrabromomethane (3.0 g, 9.0 mmol, 12 equiv), and triphenylphosphine (2.4 g, 9.0 mmol, 12 equiv), dried DCM (50 mL) was added, and the reaction mixture was stirred for overnight at room temperature under argon atmosphere. The compound 4 (300 mg, 0.75 mmol, 1.0 equiv) was added, and the reaction mixture was stirred for 2 h at room temperature. The resulting mixture was filtrated through a short pad of silica with DCM, and the crude product was used without further purification in the next step. To dried tetrahydrofuran (7.5 mL) and diisopropylamine (1.2 mL, 8.3 mmol, 11 equiv), n-butyllithium solution (2.5 M in n-hexane, 3.3 mL, 8.3 mmol, 11 equiv) was added at -78° C dropwise. The reaction mixture was stirred for 1 h at -78° C under the argon atmosphere. After 1 h, the crude compound of the previous step (1.0 equiv) solution in tetrahydrofuran (22.5 mL) was added to a lithium diisopropylamide (LDA) solution at -78° C dropwise. The reaction mixture was stirred for 10 min at -78°C under the argon atmosphere. Saturated ammonium chloride solution (7.5 mL) was added, and the reaction mixture was stirred until the temperature raised room temperature. The resulting mixture was extracted with n-hexane (25 mL \times 3) and water (25 mL). The combined organic layer was dried over anhydrous sodium sulfate and concentrated in vacuo. The crude product was purified by adsorption column chromatography (n-hexane) to obtain desired product 1 (250 mg; 86% yield for the two steps) as white solid.

Synthesis of HGY

The interface method between two immiscible liquids was used for the synthesis of HGY. The upper aqueous solvent layer (10 mL deionized [DI] water) included the copper acetate (CuOAc) and pyridine, which acted as a catalyst for the acetylenic homocoupling. ^{14,30} Then, a DI water (10 mL) layer was added in the middle as the buffer layer, making the reaction circumvent the random encounter between monomer 1 and the catalyst. The lower organic layer of DCM (10 mL) includes monomer 1. All these processes kept the carbon-carbon coupling reaction for 48 h under an inert argon atmosphere at room temperature. The HGY was cleaned with each pure DCM and then DI water several times. Finally, HGY was transferred to the substrate, such as a silicon wafer.

DFT calculations

All calculations were carried out based on DFT 31,32 using the Vienna Ab initio Simulation Package (VASP) code. The projector-augmented wave (PAW) method was used to describe the ion-electron interaction. For the following calculations of properties, generalized gradient approximation (GGA) with the Perdew-Burke-Ernzerhof (PBE) functional was used to describe the exchange-correlation potential. The $5 \times 5 \times 1$ and $11 \times 11 \times 1$ Monkhorst-Pack F points were used for geometry optimizations and self-consistent calculations, respectively. The electronic wave functions were expanded using a plane-wave basis set with a cutoff energy of 500 eV. All structural models were entirely relaxed until the ionic Hellmann-Feynman forces were smaller than 10^{-6} eV/Å, and the energy tolerances were less than 10^{-6} eV/atom.

To examine the dynamic stability of HGY, the phonon dispersion was calculated by combining the VASP with phonopy code. 36 The 4 × 4 × 1 Monkhorst-Pack K points

Please cite this article in press as: Liu et al., Constructing two-dimensional holey graphyne with unusual annulative π -extension, Matter (2022), https://doi.org/10.1016/j.matt.2022.04.033





were determined during the calculation of force constants. We also performed AIMD simulations to evaluate thermal stability using the VASP code. 37 In the AIMD simulations, the 2 × 2 × 1 supercell was annealed at 1,000 K for a period of 10 ps with a time step of 2.0 fs with NVT canonical ensemble methods. The band structure used the PBE 38 functional that tends to underestimate the bandgap of materials and Heyd-Scuseria-Ernzerhof (HSE06) 39 screened-hybrid functional that was proven to be a reliable method for the calculation of electronic properties.

Further information on the experimental and computational methods is provided in the supplemental information.

SUPPLEMENTAL INFORMATION

Supplemental information can be found online at https://doi.org/10.1016/j.matt. 2022.04.033.

ACKNOWLEDGMENTS

This work was supported in Korea by the Institute for Basic Science (IBS-R011-D1) and was supported in part by Advanced Facility Center for Quantum Technology, National Research Foundation of Korea (NRF) grants (no. 2019R1A4A2001440) and in USA by the NSF Centre for the Advancement of Wearable Technologies (grant 1849243) and by NASA (grant number 80NSSC19M0236). X.L. thanks Prof. Zhigang Shuai and Jinyang Xi for their helpful discussion. We thank Prof. Munseok Jeong group for the Raman measurement and discussion about the Raman data. X.L. thanks Suar Oh for taking AFM measurement and Yeseul Hong for taking the SEM measurement.

AUTHOR CONTRIBUTIONS

X.L., D.H.R., and H.L. conceived the idea and directed the project. X.L. designed and synthesized holey graphyne, the structure, and spectroscopic analysis. S.M.C. synthesized 1,3,5-tribromo-2,4,6-triethynylbenzene. X.L., S.L., and Z.C. performed DFT studies. W.C. and Y.-M.K. conducted HRTEM experiments and simulations. E.Y. and E.H.B. gave the help for the experimental part of the holey graphyne and 1,3,5-tribromo-2,4,6-triethynylbenzene, respectively. X.L. and H.L. wrote the original draft. All of the authors discussed the results and wrote the paper.

DECLARATION OF INTERESTS

The authors declare no competing interests.

Received: January 26, 2022 Revised: March 15, 2022 Accepted: April 26, 2022 Published: May 18, 2022

REFERENCES

- Novoselov, K.S., Geim, A.K., Morozov, S.V., Jiang, D., Zhang, Y., Dubonos, S.V., Grigorieva, I.V., and Firsov, A.A. (2004). Electric field effect in atomically thin carbon films. Science 306, 666–669. https://doi.org/10.1126/science. 1102896.
- Kroto, H.W., Heath, J.R., O'Brien, S.C., Curl, R.F., and Smalley, R.E. (1985). C60: buckminsterfullerene. Nature 318, 162–163. https://doi.org/10.1038/318162a0.
- 3. lijima, S. (1991). Helical microtubules of graphitic carbon. Nature 354, 56–58. https://doi.org/10.1038/354056a0.
- Li, G., Li, Y., Liu, H., Guo, Y., Li, Y., and Zhu, D. (2010). Architecture of graphdiyne nanoscale films. Chem. Commun. 46, 3256–3258. https://doi.org/10.1039/b922733d.
- 5. Baughman, R.H., Eckhardt, H., and Kertesz, M. (1987). Structure-property predictions for
- new planar forms of carbon: layered phases containing sp² and sp atoms. J. Chem. Phys 87, 6687–6699. https://doi.org/10.1063/1. 453405.
- Malko, D., Neiss, C., Viñes, F., and Görling, A. (2012). Competition for graphene: graphynes with direction-dependent Dirac cones. Phys. Rev. Lett. 108, 086804. https://doi.org/10.1103/physrevlett.108. 086804.

Matter Article



- Wu, W., Guo, W., and Zeng, X.C. (2013). Intrinsic electronic and transport properties of graphyne sheets and nanoribbons. Nanoscale 5, 9264–9276. https://doi.org/10.1039/ C3NR03167E.
- Li, Y., Xu, L., Liu, H., and Li, Y. (2014). Graphdiyne and graphyne: from theoretical predictions to practical construction. Chem. Soc. Rev. 43, 2572–2586. https://doi.org/10. 1039/C3C560388A.
- Gao, X., Liu, H., Wang, D., and Zhang, J. (2019). Graphdiyne: synthesis, properties, and applications. Chem. Soc. Rev. 48, 908–936. https://doi.org/10.1039/C8CS00773J.
- Rabia, A., Tumino, F., Milani, A., Russo, V., Bassi, A.L., Bassi, N., Lucotti, A., Achilli, S., Fratesi, G., Manini, N., et al. (2020). Structural, electronic, and vibrational properties of a twodimensional graphdiyne-like carbon nanonetwork synthesized on au (111): implications for the engineering of sp-sp² carbon nanostructures. ACS Appl. Nano Mater. 3, 12178–12187. https://doi.org/10.1021/ acsanm 0c02665.
- Serafini, P., Milani, A., Proserpio, D.M., and Casari, C.S. (2021). Designing all graphdiyne materials as graphene derivatives: topologically driven modulation of electronic properties. J. Phys. Chem. C 125, 18456–18466. https://doi.org/10.1021/acs.jpcc.1c04238.
- Novoselov, K.S., Fal'ko, V.I., Colombo, L., Gellert, P.R., Schwab, M.G., and Kim, K. (2012). A roadmap for graphene. Nature 490, 192–200. https://doi.org/10.1038/nature11458.
- Wong, H.N.C., Garratt, P.J., and Sondheimer, F. (1974). Unsaturated eight-membered ring compounds. XI. Synthesis of sym-dibenzo-1,5cyclooctadiene-3,7-diyne and sym-dibenzo-1,3,5-cyclooctatrien-7-yne, presumably planar conjugated eight-membered ring compounds. J. Am. Chem. Soc. 96, 5604–5605. https://doi. org/10.1021/ja00824a066.
- Stephens, R.D., and Castro, C.E. (1963). The substitution of aryl iodides with cuprous acetylides. A synthesis of tolanes and Heterocyclics. J. Org. Chem. 28, 3313–3315. https://doi.org/10.1021/jo01047a008.
- Becker, M., Voss, K., Villinger, A., and Schulz, A. (2012). An efficient route to 1, 3, 5-triazido-2, 4, 6-tricyanobenzene. Z. Naturforsch. 67, 643–649. https://doi.org/10.5560/znb.2012-0092.
- Corey, E.J., and Fuchs, P.A. (1972). A synthetic method for formyl → ethynyl conversion (RCHO → RC CH or RC CR'). Tetrahedron Lett. 13, 3769–3772. https://doi.org/10.1016/S0040-4039(01)94157-7.

- Reina, A., Jia, X., Ho, J., Nezich, D., Son, H., Bulovic, V., Dresselhaus, M.S., and Kong, J. (2009). Large area, few-layer graphene films on arbitrary substrates by chemical vapor deposition. Nano Lett. 9, 30–35. https://doi. org/10.1021/nl801827v.
- Zhou, J., Gao, X., Liu, R., Xie, Z., Yang, J., Zhang, S., Zhang, G., Liu, H., Li, Y., Zhang, J., and Liu, Z. (2015). Synthesis of graphdiyne nanowalls using acetylenic coupling reaction. J. Am. Chem. Soc. 137, 7596–7599. https://doi. org/10.1021/jacs.5b04057.
- Qian, X., Liu, H., Huang, C., Chen, S., Zhang, L., Li, Y., Wang, J., and Li, Y. (2015). Self-catalyzed growth of large-area nanofilms of twodimensional carbon. Sci. Rep. 5, 7756. https:// doi.org/10.1038/srep07756.
- Park, C., Ryou, J., Hong, S., Sumpter, B.G., Kim, G., and Yoon, M. (2015). Electronic properties of bilayer graphene strongly coupled to interlayer stacking and an external electric field. Phys. Rev. Lett. 115, 015502. https://doi. org/10.1103/PhysRevLett.115.015502.
- Cao, Y., Fatemi, V., Demir, A., Fang, S., Tomarken, S.L., Luo, J.Y., Sanchez-Yamagishi, J.D., Watanabe, K., Taniguchi, T., Kaxiras, E., et al. (2018). Correlated insulator behaviour at half-filling in magic-angle graphene superlattices. Nature 556, 80–84. https://doi. org/10.1038/nature25154.
- Liu, X., Hao, Z., Watanabe, K., Taniguchi, T., Halperin, B.I., and Kim, P. (2019). Interlayer fractional quantum Hall effect in a coupled graphene double layer. Nat. Phys. 15, 893–897. https://doi.org/10.1038/s41567-019-0546-0.
- Tuinstra, F., and Koenig, J.L. (1970). Raman spectrum of graphite. J. Chem. Phys. 53, 1126– 1130. https://doi.org/10.1063/1.1674108.
- Matsuoka, R., Sakamoto, R., Hoshiko, K., Sasaki, S., Masunaga, H., Nagashio, K., and Nishihara, H. (2017). Crystalline graphdiyne nanosheets produced at a gas/liquid or liquid/ liquid interface. J. Am. Chem. Soc. 139, 3145– 3152. https://doi.org/10.1021/jacs.6b12776.
- Long, M., Tang, L., Wang, D., Li, Y., and Shuai, Z. (2011). Electronic structure and carrier mobility in graphdiyne sheet and nanoribbons: theoretical predictions. ACS Nano 5, 2593– 2600. https://doi.org/10.1021/nn102472s.
- Bardeen, J., and Shockley, W. (1950).
 Deformation potentials and mobilities in non-polar crystals. Phys. Rev. 80, 72–80. https://doi.org/10.1103/PhysRev.80.72.
- Cai, Y., Zhang, G., and Zhang, Y.-W. (2014). Polarity-reversed robust carrier mobility in monolayer MoS₂ nanoribbons. J. Am. Chem. Soc. 136, 6269–6275. https://doi.org/10.1021/ ja4109787.

- Lin, S., Gu, J., Wang, Y., Wang, Y., Zhang, S., Liu, X., Zeng, H., and Chen, Z. (2018). Porous silaphosphorene, silaarsenene and silaantimonene: a sweet marriage of Si and P/As/Sb. J. Mater. Chem. A. 6, 3738–3746. https://doi.org/10.1039/C7TA10466A.
- Chen, J., Xi, J., Wang, D., and Shuai, Z. (2013). Carrier mobility in graphyne should be even larger than that in graphene: a theoretical prediction. J. Phys. Chem. Lett. 4, 1443–1448. https://doi.org/10.1021/jz4005587.
- Eglinton, G., and Galbraith, A.R. (1959). Macrocyclic acetylenic compounds. Part I. Cyclotetradeca-1: 3-diyne and related compounds. J. Chem. Soc. 182, 889–896. https://doi.org/10.1039/JR9590000889.
- Kresse, G., and Furthmüller, J. (1996). Efficiency of ab-initio total energy calculations for metals and semiconductors using a plane-wave basis set. Comput. Mater. Sci. 6, 15–50. https://doi. org/10.1016/0927-0256(96)00008-0.
- Kresse, G., and Furthmüller, J. (1996). Efficient iterative schemes for ab initio total-energy calculations using a plane-wave basis set. Phys. Rev. B 54, 11169–11186. https://doi.org/10. 1103/physrevb.54.11169.
- Kresse, G., and Joubert, D. (1999). From ultrasoft pseudopotentials to the projector augmented-wave method. Phys. Rev. B 59, 1758–1775. https://doi.org/10.1103/PhysRevB. 59.1758.
- Perdew, J.P., Burke, K., and Ernzerhof, M. (1996). Generalized gradient approximation made simple. Phys. Rev. Lett. 77, 3865–3868. https://doi.org/10.1103/PhysRevLett.77.3865
- Monkhorst, H.J., and Pack, J.D. (1976). Special points for Brillouin-zone integrations. Phys. Rev. B 13, 5188–5192. https://doi.org/10.1103/ PhysRevB.13.5188.
- Togo, A., and Tanaka, I. (2015). First principles phonon calculations in materials science. Scr. Mater. 108, 1–5. https://doi.org/10.1016/j. scriptamat.2015.07.021.
- Andersen, H.C. (1980). Molecular dynamics simulations at constant pressure and/or temperature. J. Chem. Phys. 72, 2384–2393. https://doi.org/10.1063/1.439486.
- Filippi, C., Singh, D.J., and Umrigar, C.J. (1994). All-electron local-density and generalizedgradient calculations of the structural properties of semiconductors. Phys. Rev. B 50, 14947–14951. https://doi.org/10.1103/ physrevb.50.14947.
- Heyd, J., Scuseria, G.E., and Ernzerhof, M. (2003). Hybrid functionals based on a screened coulomb potential. J. Chem. Phys. 118, 8207– 8215. https://doi.org/10.1063/1.1564060.